Supplement of Atmos. Chem. Phys., 23, 8271–8304, 2023
https://doi.org/10.5194/acp-23-8271-2023-supplement

Atmospheric Chemistry and Physics
Open Access

Supplement of

Thermal infrared dust optical depth and coarse-mode effective diameter over oceans retrieved from collocated MODIS and CALIOP observations

Jianyu Zheng et al.

Correspondence to: Zhibo Zhang (zzbatmos@umbc.edu)

1 The *a priori* monomodal lognormal volume size distribution

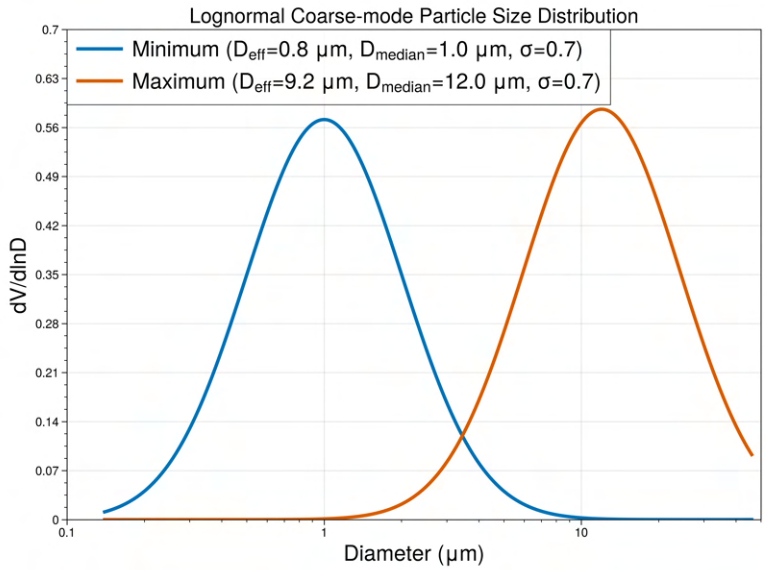

Figure S1: The assumed dust monomodal coarse-mode volume size distribution with the geometric volume median diameter ranging from 1.0 µm to 12.0 µm, the fixed standard deviation at 0.7, and the effective diameter ranging from 0.8 µm to 9.2 µm.

2 The refractive index assignment based on the dust source fractional contribution from DustCOMM

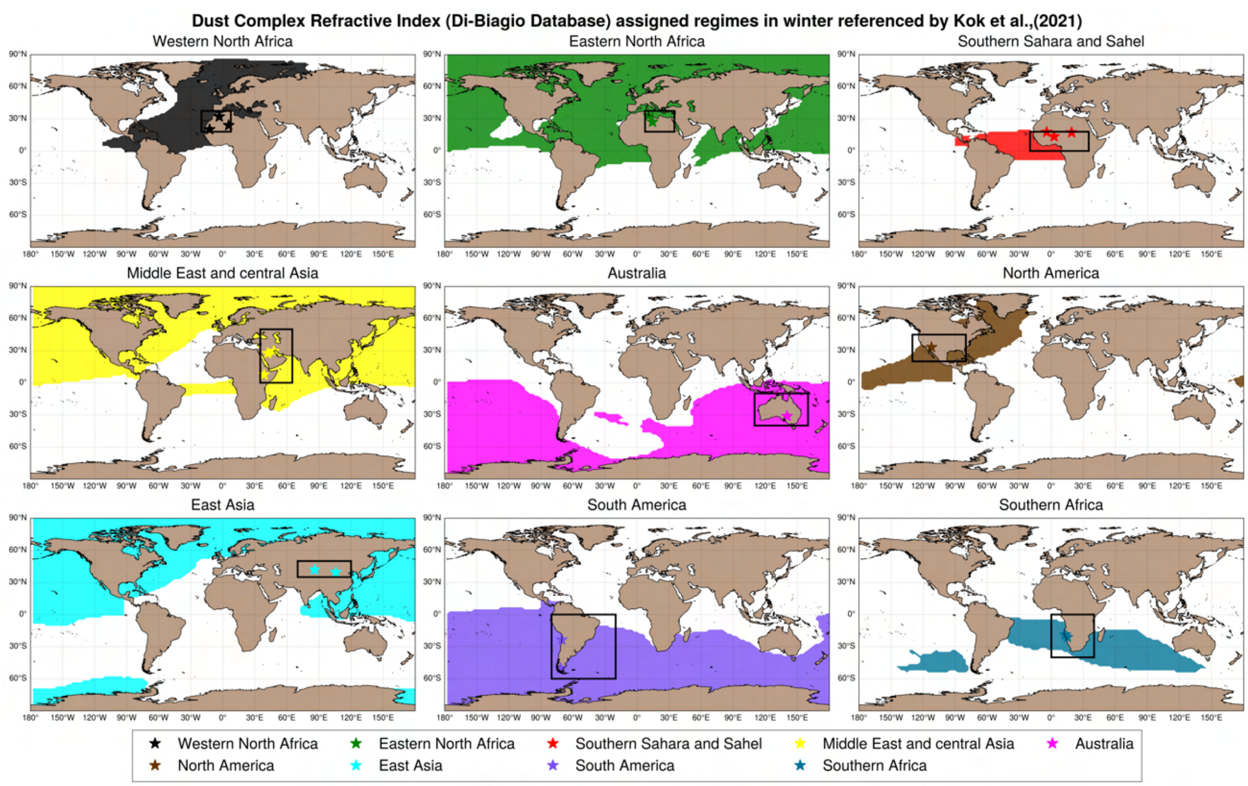

Figure S2: The assignment of the source region-resolved dust refractive indices from Di Biagio et al. (2017) is based on which of the nine main source regions provided a fractional contribution to SW DAOD that exceeds 0.1, which is shown here for winter based on the DustCOMM-2021 dataset.

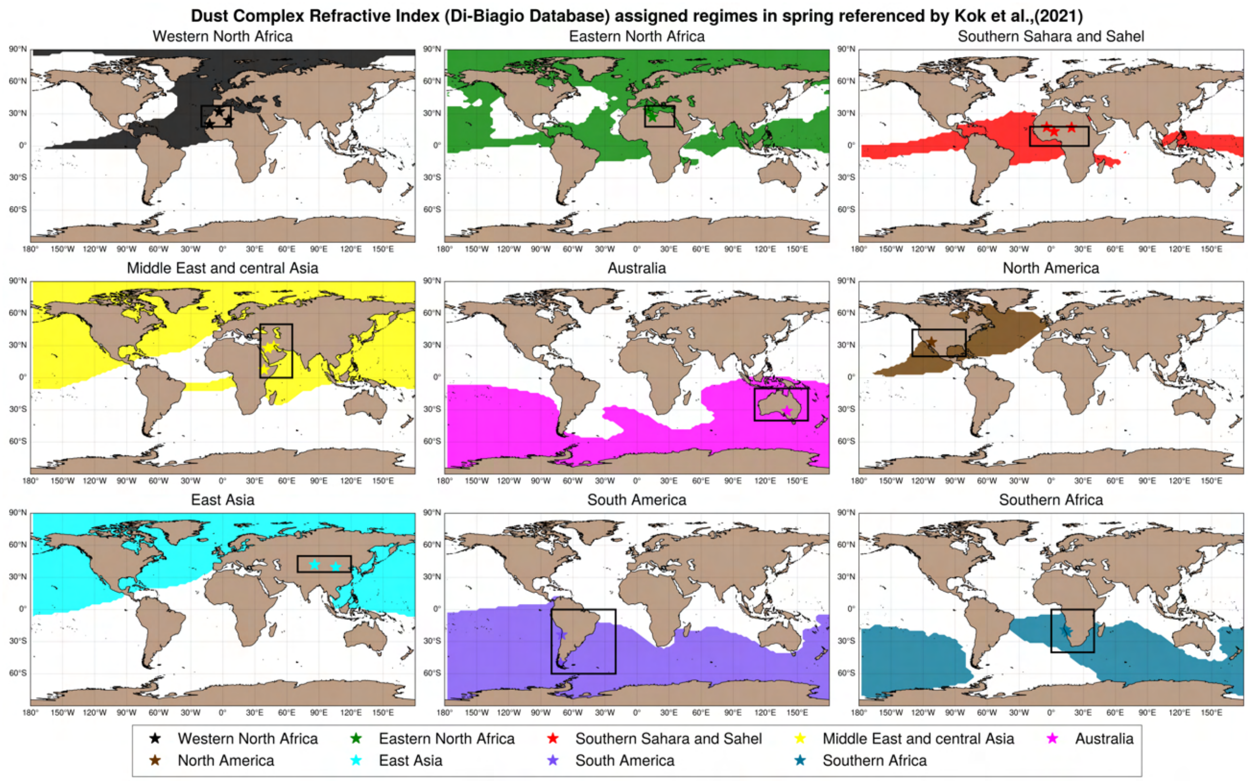

Figure S3: Same as Figure S2 but for spring based on the DustCOMM-2021 dataset.

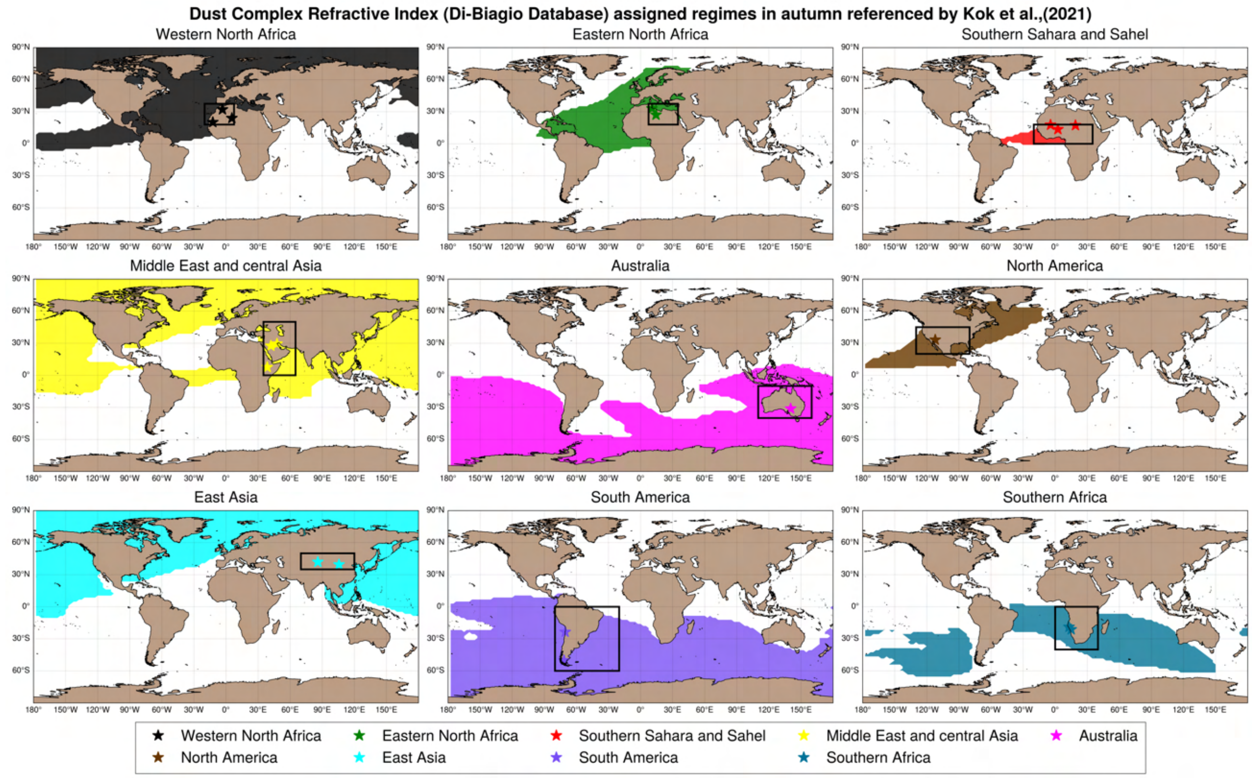

Figure S4: Same as Figure S2 but for autumn based on the DustCOMM-2021 dataset.

3 The sensitivity of TIR radiative signature to the σ of dust particle size distributions and dust refractive indices

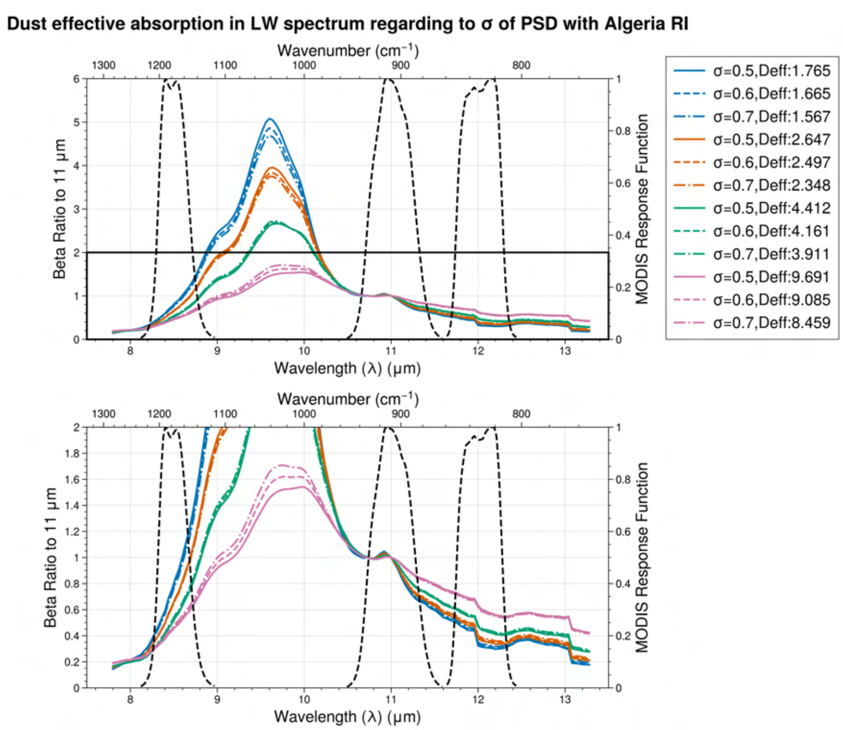

Figure S5: (a) The β-ratio to 11 μm calculated based on D_m = 2 μm (blue), 3 μm (red), 5 μm (green) and 10 μm (pink) with three different σ (i.e., σ = 0.5 (real curves), 0.6 (dash curves), 0.7 (dot-dash curves)) of dust PSD and the Algeria dust RI

from Di-Biagio Database within the TIR spectrum between 7.5 µm and 13.5 µm. (b) The zoom-in area of the black rectangle in (a).

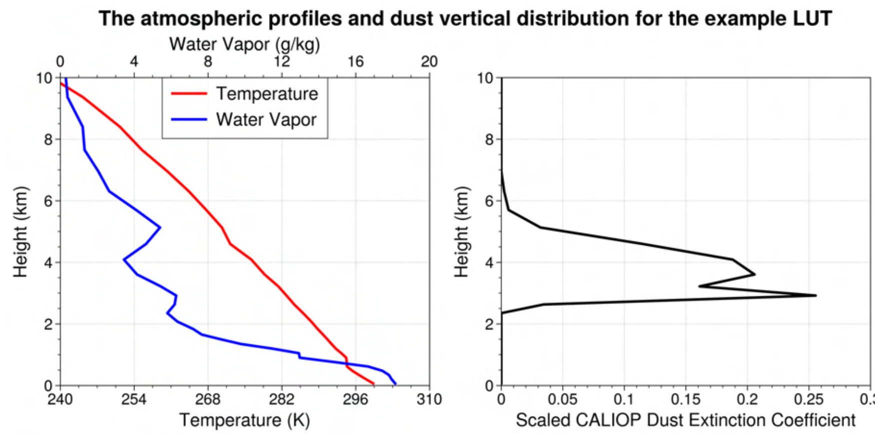

Figure S6: The atmospheric profile and dust vertical distribution used for building the LUT in Figure 4 and LUTs in Figures S7 and S8.

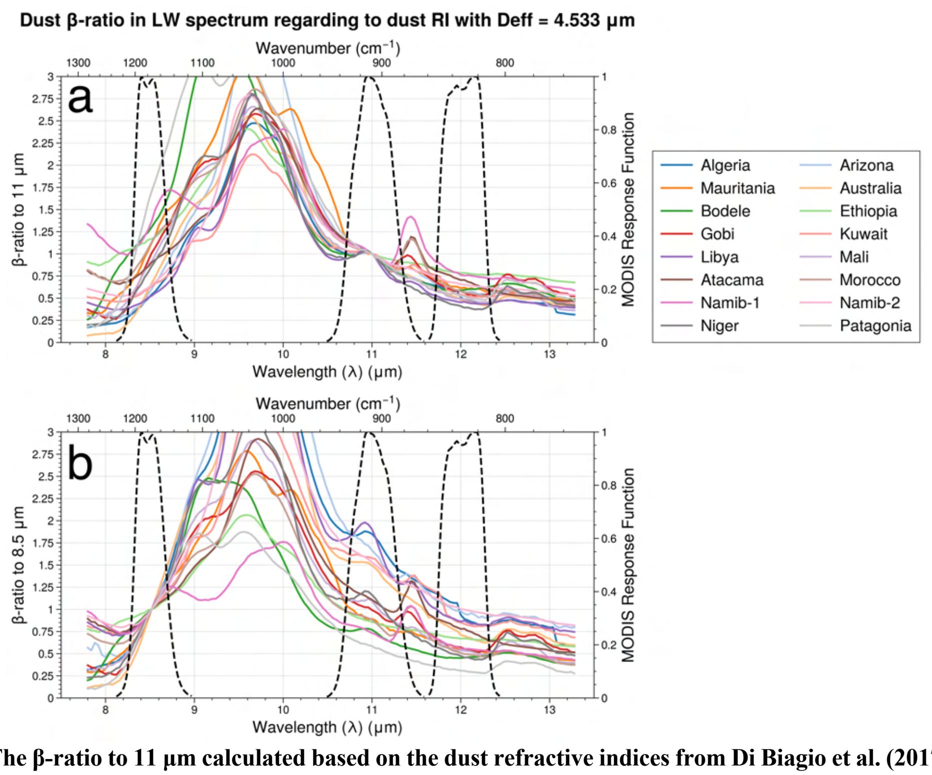

Figure S7: (a) The β-ratio to 11 µm calculated based on the dust refractive indices from Di Biagio et al. (2017) and D_{eff} = 4.5 µm within the TIR spectrum between 7.5 µm and 13.5 µm. (b) Same as (a) but the β-ratio to 8.5 µm.

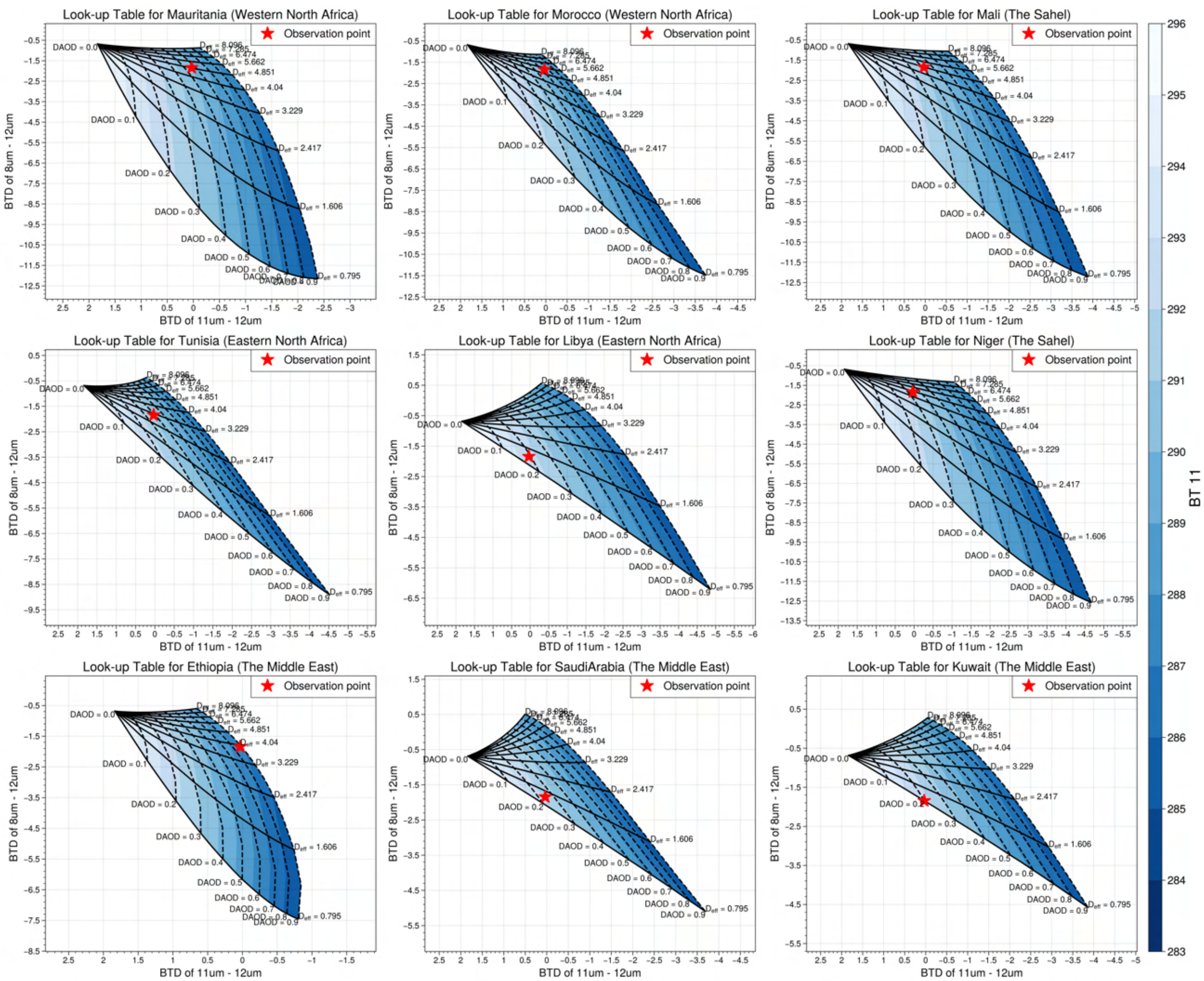

Figure S8: The example of the LUT of BTD_{8-12} (y-axis), BTD_{11-12} (x-axis) and BT_{11} (colour-filled contours) corresponding to DAOD at 10 µm ranging from 0.0 to 1.0 (dashed lines) and D_{eff} ranging from 0.8 µm to 9.0 µm (solid lines) and eighteen dust RIs except the Algeria RI (Figure 2a) from Di-Biagio Database. At DAOD = 0.0, the BTD_{8-12} and BTD_{11-12} correspond to the cloud-free clean scenario. The red dots represent an identical assumed observation point projected on the nine LUTs, leading to different retrieval solutions.

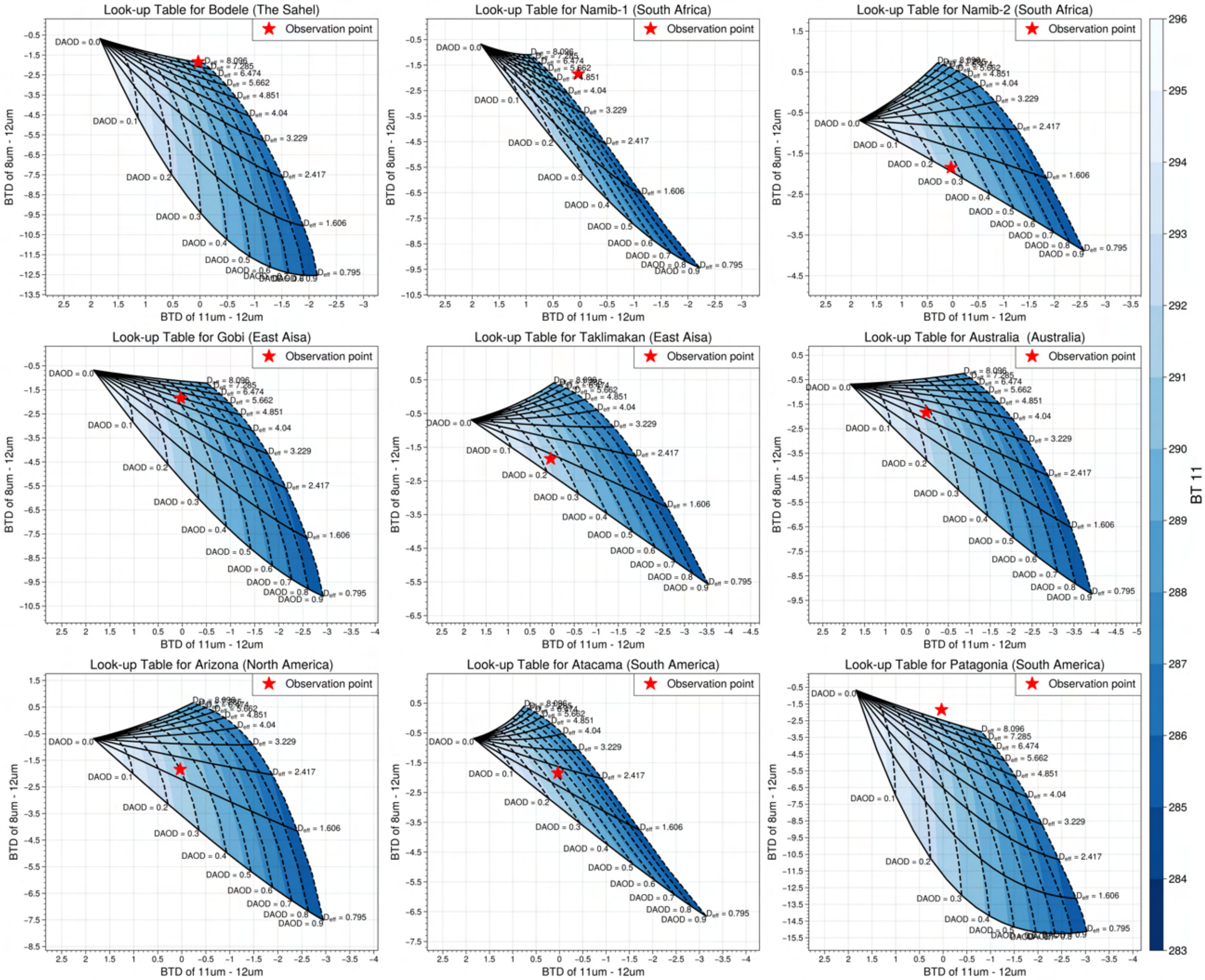

Figure S9: Continued as Figure S7.

4 The sample distributions of the retrieval from 2013 to 2017

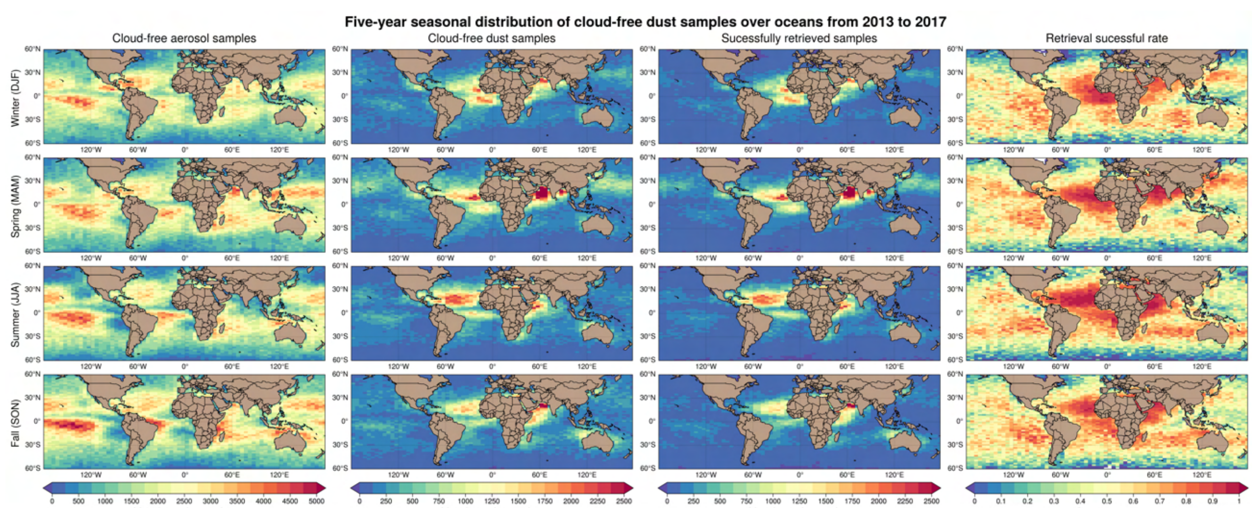

Figure S10: The five-year global seasonal distribution in a 5° longitude by 2° latitude resolution of the cloud-free aerosol samples ($N_{aerosol}$; left column), the cloud-free aerosol samples (N_{dust}; middle-left column), the successfully retrieved samples ($N_{retrieval}$; middle-right column) and the retrieval success rate ($N_{retrieval}$ / N_{dust}; right column). From the top row to the bottom presents seasons from winter to fall.